

AstroSat and *Insight–HXMT* observations of the long-period X-ray pulsar 4U 2206+54

PRAHLAD R. EPILI¹ AND WEI WANG¹

¹*Department of Astronomy, School of Physics and Technology, Wuhan University, Wuhan 430072, China P.R.C**

ABSTRACT

We report the timing and spectral studies of the accreting X-ray pulsar 4U 2206+54 using *AstroSat* and *Insight–HXMT* observations taken in 2016 and 2020 respectively. X-ray pulsations from the system are detected by both missions. The *AstroSat* discovered a significant periodic signal at ~ 5619 s in 2016 and *Insight–HXMT* found a pulsation period at ~ 5291 s in 2020. A comparison of its spin-period evolution with the present spin-period estimates shows that the neutron star in 4U 2206+54 now has recently undergoing a spin-up episode after attaining to its slow pulsations of 5750 s around 2015 from its prolonged spin-down phase. The present average spin-up rate of the pulsar is found to be at $\sim 1.2 \times 10^{-13}$ Hz s⁻¹. The phase-averaged spectra of the pulsar in 1–60 keV could be explained with a high energy cutoff power-law continuum model, no evident line features are found with *AstroSat*. The application of Comptonization models such as *COMP*TT and *COMP*MAG to the phase averaged spectra of 4U 2206+54 reveal a hotter source photon region near the pulsar with an emission size extending to $\sim 2 - 2.8$ km. Using the quasi-spherical settling accretion theory, we explain the present spin-up and the possibility of strong magnetic field of the pulsar.

Keywords: stars: magnetic field –stars: neutron –pulsars: individual: 4U 2206+54 –X-rays: binaries

1. INTRODUCTION

4U 2206+54 is a persistent low luminosity ($\sim 10^{35}$ erg s⁻¹) high mass X-ray binary (HMXB) system consisting of a neutron star orbiting an O-type companion star. The neutron star in this system is known to show long period pulsations of ~ 5550 sec (Reig et al. 2009; Finger et al. 2010; Wang 2010, 2013). Along with 2S 0114+650, GX 301–2, IGR J16358–4726 and X Per it belongs to a peculiar family of HMXB sources (Blay & Reglero 2012; Blay et al. 2014) in which the NS pulse period is longer than 100s of seconds, has a persistent low luminosity, accretes from the slow and dense stellar wind of companion star and NS shows long-term spin down trend since 2000 (Wang 2013).

4U 2206+54 remains till date, an exceptional member of high mass X-ray binary systems. Although it was identified as an X-ray source since more than 20 years ago, the nature of the compact object remained uncertain until Reig et al. (2009) found a ~ 5560 s modulation in the X-ray light curve of the source. It was later understood as spin period of the neutron star. The findings of slow pulsations have put an end to the long standing debate on the nature of compact object in 4U 2206+54. However, it posed new challenges in classifying the source in either subgroups of HMXBs. The optical companion in 4U 2206+54 is a main-sequence O9.5V star

having excess in He abundance which suggests against the supergiant X-ray binary classification. The X-ray light curve of 4U 2206+54 also differs from majority of Be/X-ray binaries (Reig et al. 2012) in a way that there are no Type-I X-ray outbursts or any aperiodic giant Type II outbursts (without any modulations on the orbital period). The X-ray emission from the source is understood to be due to accretion of slow and dense wind from the non-supergiant companion star. As per spin-evolutionary models in close binaries, the slow pulsations found in 4U 2206+54 imply its surface magnetic field value of the order $\geq 10^{14}$ G. This would lead to assumption that the X-ray source in 4U 2206+54 binary system is an accreting magnetar (Finger et al. 2010).

Since its discovery with *Uhuru* in 1972, 4U 2206+54 is observed with various X-ray observatories. From the earliest ~ 9 ks *RXTE* PCA observations of 4U 2206+54 (i.e. March 1997), it was reported that the temporal X-ray variability of the source is associated with flaring activity on short time scales (Negueruela & Reig 2001). The X-ray intensity was varying by a factor of 3 within 2 minutes. 4U 2206+54 was also caught in a hard X-ray outburst during December 2005 with *INTEGRAL/IBIS*. The hard X-ray outburst had double-flare events lasting for 2-days. The first flare was seen with a peak luminosity of $\sim 4 \times 10^{36}$ erg s⁻¹ in 1.5–12 keV range whereas the second flare had an average X-ray luminosity of 1.3×10^{36} erg s⁻¹ in 20–150 keV energy band (Wang 2010). The reported bright flares are similar to those found in SFXTs

* Email address: prahlad@whu.edu.cn, wangwei2017@whu.edu.cn

but the physical mechanisms responsible for sudden and enhanced wind accretion in 4U 2206+54 remains speculative. It was further suggested that the accreting material in the form of clumps from the stellar wind could hit the polar cap region of neutron star in 4U 2206+54 leading to hard X-ray outbursts. Hence a detailed study is required to understand the various effects on accretion through the capture of stellar wind of a main sequence star in 4U 2206+54 and thereby providing the missing link between these systems and SFXTs (Wang 2010).

The evolutionary trend of slow pulsation period (*i.e.* longer than 5000 s) and origin of X-ray variability in 4U 2206+54 remain poorly understood. Since 4U 2206+54 is one of the weak and low-luminosity hard X-ray source and the available observations are relatively short, there exists a large uncertainty in determining the spin period and period derivative for the pulsar. Long pulsation period (~ 5560 s) of 4U 2206+54 makes it one of the accreting X-ray pulsar with slowest pulsations. According to standard models of spin-period evolution of young neutron star in close binary systems, the newborn neutron star goes through three primary stages of evolution (Bhattacharya & van den Heuvel 1991) before being switched on as an X-ray pulsar. In the first stage *i.e. ejector state*, the neutron star loses rotational energy through spinning down. In the *propeller state*, the spin period of the neutron star decreases due to interaction between its magnetosphere and the stellar wind of the companion. In *accretor state*, the neutron star starts accreting material on to the surface when its spin period reaches a critical value. From then onwards, it beams X-ray emissions as an X-ray pulsar. The spin period of the neutron star during *ejector* and *propeller* states could only increase to the longest period of several hundred seconds but cannot be more than 1000 s (Urpin et al. 1998; Wang 2013). Hence, the very slow pulsations of period longer than 5000 s found in 4U 2206+54 could not be explained in this standard picture (Wang 2013). So, the evolution pathway of these slow pulsar is still unknown and remains quiet an interesting topic in astrophysics.

Detection of cyclotron lines in the spectra of accretion powered X-ray pulsars gives us a direct estimate of neutron star surface magnetic field. In 4U 2206+54, a tentative detection of cyclotron resonance scattering feature (CRSF) near ~ 30 keV has been reported in past by *RXTE*, *BeppoSAX* and *INTEGRAL* observations at different epochs between 1997 and 2005 (Torrejón et al. 2004; Wang 2009). However there was no sign of any CRSF detected from a long *RXTE* observation (~ 137 ks exposure) in May 2007 (Reig et al. 2009). From the *BeppoSAX* and *Suzaku* observations, the spin-down rate of the pulsar was reported to be $\dot{\nu} = (-1.5 \pm 0.2) \times 10^{-14}$ Hz s^{-1} (Finger et al. 2010). which would imply a magnetic field of $B \sim 10^{14}$ G and hence the corresponding electron cyclotron line would appear at around

$E > 500$ keV which is beyond the range of available detectors. However, the estimated spin-down rate is based only on two observations of the pulsar. In our present work, we have discussed the *AstroSat* and *Insight-HXMT* observations of 4U 2206+54 taken in September 2016 and October 2020 respectively. In brief, the paper is structured as follows: in Section 2, we present the observation details. In Section 3, we have analysed the light-curves of 4U 2206+54 in various energy ranges. Subsequent spin-period estimation and pulse-profiles studies have been carried out. The spectral study, in particular the phase-averaged spectroscopy from *AstroSat* observations of 4U 2206+54 has been presented in Section 4 with the best-fitted empirical and physics-based models. And lastly in Sections 5 and 6, we discuss the spectral parameter variations in the prevailing theoretical frameworks and present the conclusions, respectively.

2. OBSERVATIONS AND DATA ANALYSIS

2.1. AstroSat

AstroSat (Singh et al. 2014) is India's first space observatory capable of observing the stellar sources in multi-wavelengths. It has been launched on September 28, 2015 carrying onboard five sets of scientific instruments. These are namely, a Soft X-ray Telescope (SXT, Singh et al. 2016, 2017), the Large Area X-ray Proportional Counters (LAXPC, Agrawal et al. 2017; Yadav et al. 2016), a Cadmium Zinc Telluride Imager (CZTI, Bhalerao et al. 2017; Rao et al. 2017a), a Scanning Sky Monitor (SSM, Ramadevi et al. 2017a,b) and an Ultraviolet Imaging Telescope (UVIT, Tandon et al. 2017). Also there is a Charged Particle Monitor (CPM, Rao et al. 2017b) onboard *AstroSat* to monitor the charged particle count rate variation. As the satellite passes through the SAA region, the CPM helps in optimizing the operation time of the X-ray detectors and effectively switching off these instruments during SAA passage to avoid the adverse effects on the X-ray detectors and their subsequent saturation.

The array of LAXPC detectors onboard *AstroSat* covers an energy range of 3-80 keV with a large collection area of ~ 6000 cm² at 15 keV (Yadav et al. 2016). It consists of 3 independent and identical units of proportional counter detectors (LAXPC-10, 20 & 30) working simultaneously in different modes. The default operation modes of LAXPC are: (a) Broad Band Counting of data (*i.e.* BB mode) and (b) Event Analysis mode data (*i.e.* EA mode). The Soft X-ray Telescope (SXT, Singh et al. 2016) onboard *AstroSat* is sensitive to soft X-rays in 0.3 – 8 keV energy range. The total field of view (FOV) of SXT is $\sim 40'$ with an effective area that varies from ~ 128 cm² at 1.5 keV to ~ 20 cm² at 6 keV. The hard X-ray coverage onboard *AstroSat* is provided with the Cadmium Zinc Telluride Imager (CZTI, Rao et al. 2017a; Bhalerao et al. 2017) in 20-200 keV. Its a 2D coded mask imager with The coded aperture mask on CZTI with a field of

view of $4.6 \text{ deg} \times 4.6 \text{ deg}$ (FWHM) provides $8''$ resolution for bright sources. The energy resolution of *CZTI* is of $\sim 11\%$ at 60 keV .

4U 2206+54 has been observed with *LAXPC*, *SXT*, & *CZTI* instruments onboard *AstroSat* on two occasions (*i.e.* on 06-09-2016 and 08-10-2016) respectively with observation IDs: 9000000644, 9000000720. The effective exposure of the first observation with *LAXPC* is $\sim 43.7 \text{ ksec}$. Whereas the second observation has an effective exposure of 40.7 ksec with *LAXPC* detectors. The observations are also carried simultaneously with *SXT* & *CZTI* instruments. A log of these observations used in our study are given in Table 1. In Figure 1, we show the long-term *Swift* /BAT light curve of 4U 2206+54 in 15–50 keV. The epochs of *AstroSat* observations of 4U 2206+54 used in the paper are shown with arrows in the figure. In the present work we have used the data from both of these observations to study the X-ray spectrum in 1–60 keV. For the X-ray timing studies we have used the *AstroSat* observations in energy range: 0.3–5 keV from *SXT*, 5–30 keV from *LAXPC* and 30–60 keV from *CZTI* observations of 4U 2206+54 respectively.

2.1.1. SXT Observations

The SXT observations of 4U 2206+54 were carried out as a Regular Pointings in Photon Counting (PC) mode with a total on source effective exposure of $\sim 26.1 \text{ ks}$ during the *AstroSat* orbits 5574 (MJD 57669.67) to 5589 (MJD 57670.69) (excluding the orbit-wise overlap of 3.9 ks). We have obtained the SXT level-2 data of our source from *ISRO Science Data Archive for Astrosat Mission*¹ located at ISSDC². These were processed from the level-1 data with the SXTPIPELINE version 1.4a³.

At first we have merged the available orbit wise SXT level-2 clean event data of our source using SXT Event Merger Tool.⁴ This resulted in a single clean event file with an effective exposure of $\sim 21.4 \text{ ksec}$ (from ObsID: 900000644) and $\sim 26.1 \text{ ksec}$ (from ObsID: 900000720). We have used XSELECT to extract an image of the source from the cleaned event files within the SXT field of view. We have considered a $10'$ circular region and an annular region of inner and outer radius of $13'$ & $15'$ centered at the source as the background region to obtain the source and background products (spectra, lightcurves) respectively from the *SXT* observations. We have obtained the background subtracted source light curves of 4U 2206+54 in three different energy ranges (0.3–3 keV, 3–5 keV & 5–8 keV) with the appropriate range of channel selection within XSELECT. The low energy (0.3–8 keV)

SXT spectra of 4U 2206+54 has been obtained from the SXT level-2 merged clean event file. A brief description of obtaining SXT spectra of 4U 2206+54 and its subsequent analysis has been explained in section 4.1.

2.1.2. LAXPC Observations

In the present paper, we have used the *LAXPC* observations of 4U 2206+54 carried out in Event Analysis (EA) mode for our analysis and investigating the spectral and temporal variations of source. The level-1 data from all the three *LAXPC* units corresponding to EA mode observations of 4U 2206+54 (*i.e.* having *AstroSat* OBSID:9000000720) have been obtained from the *AstroSat* data archive at ISSDC. In order to follow up the recent spin period changes in 4U 2206+54 (as described in the section 3.1), we have also used another archival *AstroSat* /*LAXPC* observation of 4U 2206+54 (Observation-ID : 9000000644). This observation has been carried out near the MJD 57637 with an effective exposure of $\sim 43.7 \text{ ks}$. A log of these observations is given in Table 1. The *AstroSat* Science Support Cell⁵ (Roy et al. 2021) provides various software packages related to *LAXPC* observations to generate level-2 event data and subsequent extraction of source spectra and light curves. Among these we have used the *LAXPC* software (August 15, 2022 version) to extract the science products from our observations.

2.1.3. CZTI Observations

In our study, the observations of 4U 2206+54 taken with *CZTI* in its Normal mode (M0) of operation are considered. A log of *CZTI* observations are shown in Table 1. The individual events recorded in this mode have a timing accuracy of $20 \mu\text{s}$. For the analysis of *CZTI* data, we have used the *cztpipeline* (version 3.0)⁶. We have followed the instructions as described in the *CZTI* analysis software user guide⁷ to process the "Level 1" data into "Level 2" standard data products. Using the *cztpipeline* module of the analysis software, we have generated the spectrum, spectral response and light curves in different energy bands for both the *AstroSat* observations of 4U 2206+54. The coded mask imager in *CZTI* also measures the background simultaneously. Using this the background-subtracted products were generated. We have used the the module *cztbdata* of the pipeline with the mask-weighting technique to produce background subtracted source light curves and spectrum.

2.2. Insight–HXMT Observations

¹ https://astrobrowse.issdc.gov.in/astro_archive/archive/Home.jsp

² <https://www.issdc.gov.in/astro.html>

³ https://www.tifr.res.in/astrosat_sxt/sxtpipeline.html

⁴ http://www.tifr.res.in/~astrosat_sxt/dataanalysis.html

⁵ <http://astrosat-ssc.iucaa.in/?q=laxpcData>

⁶ <http://astrosat-ssc.iucaa.in/cztiData>

⁷ http://astrosat-ssc.iucaa.in/uploads/czti/CZTI_analysis_software_userguide_v3.0.pdf

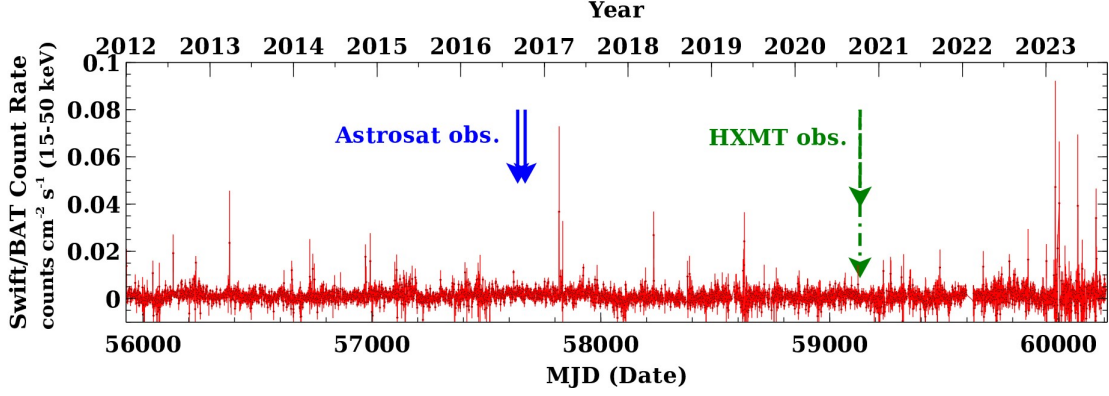


Figure 1. Swift/BAT light curve of 4U 2206+54 in 15–50 keV . The arrows indicate the respective epochs of *AstroSat* and *Insight–HXMT* observations used in the present work.

Table 1. Summary of the X-ray observations of 4U 2206+54 .

Satellite	Obs. ID	Obs. Date	Instrument	Effective Exposure (ksec)	Count-rate (cs^{-1})	Observation Mode ^a
<i>AstroSat</i>	9000000644	2016 Sept 6	SXT	21.4	~ 0.55	PC (~ 2.38 s)
			LAXPC	43.7	~ 35.05	EA ($10 \mu s$)
			CZTI	44.7	~ 1.24	M0 ($20 \mu s$)
	9000000720	2016 Oct 8	SXT	26.1	~ 1.10	PC (~ 2.38 s)
			LAXPC	40.7	~ 45.84	EA ($10 \mu s$)
			CZTI	46.3	~ 0.22	M0 ($20 \mu s$)
<i>Insight–HXMT</i>	P0305070003	2020 Oct 10	LE	32.5	~ 2.36	– (1 msec)
			ME	53.6	~ 4.40	– ($240 \mu s$)
			HE	52.0	~ 10.13	– ($4 \mu s$)
	P0305070004	2020 Oct 11	LE	14.6	~ 2.38	– (1 msec)
			ME	21.8	~ 4.43	– ($240 \mu s$)
			HE	23.4	~ 9.76	– ($4 \mu s$)

^a EA: Event Analysis, PC: Photon Counting, M0: regular event mode data. The detector resolution time is given in parentheses for corresponding observation mode.

Launched in June 2017, the Hard X-ray Modulation Telescope (a.k.a *Insight–HXMT*) (Zhang et al. 2020) consists of 3 main scientific payloads. These are Low-Energy X-ray Telescope (LE, 0.7–13 keV, Chen et al. 2020), the Medium Energy X-ray Telescope (ME, 5–30 keV, Cao et al. 2020) and the High-Energy X-ray Telescope (HE, 20–250 keV, Liu et al. 2020) for scanning and pointed observations.

4U 2206+54 has been observed with *Insight–HXMT* at two epochs during 10–11, October 2020 with observation IDs: P0305070003 and P0305070004. A log of these observations along with the effective exposures in each telescope is shown in Table 1. For the analysis of these observations, we have used HXMT Data Analysis Software Pack-

age *hxmtDas* v2.04 and the calibration database *calDB* v2.06 in our work. We have used the science data taken only with small FOV detectors from HE, ME and LE telescopes. For the data calibration, screening and to generate the high level data products such as spectra, light curves and response and background files, we have followed the instructions as mentioned in the HXMT Data Reduction Guide (v2.04)⁸. A barycentric correction is applied with the tool *hxbary* to the screened event files from all the detectors before extracting the lightcurves/spectra.

⁸ <http://hxmtweb.ihep.ac.cn/SoftDoc/496.jhtml>

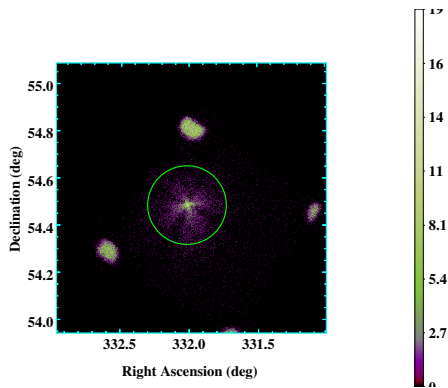


Figure 2. The soft X-ray image of the 4U 2206+54 in 0.3-7 keV within *AstroSat* /SXT FOV is shown. A circular region of 10' centered around the source is shown in green.

3. TIMING ANALYSIS

In order to study the timing variability of the long period pulsar in 4U 2206+54 and to estimate its spin period pertaining to the present observation epoch, we have extracted the source and background lightcurves from the respective level-2 event files of SXT & LAXPC observation. With the help a GTI file created (with the screening criteria as mentioned in section 2.1.2) for the LAXPC observations, we have extracted the source light curve in 3 – 80 keV with a binning of 5 sec from the LAXPC -10 unit considering all the layers. Similarly, using the script “laxpc_make_backlightcurve” provided with LAXPC software, the background lightcurves were generated for the same energy range. We performed barycentric correction to the background subtracted source light curve using the task *as1bary*. This barycentered corrected light curves of 4U 2206+54 obtained from SXT , LAXPC -1, CZTI respectively in 0.3–10 keV , 3–80 keV and 30–50 keV are shown in Fig. 3 for both the *AstroSat* observations.

From the *Insight–HXMT* observations, the background corrected and barycentered light curves of 4U 2206+54 obtained in different energy ranges as shown in Figure(s):3 and 6 for both the observations. Since each of the *Insight–HXMT* observations were segmented into exposure-IDs, we have used the FTOOLS task *ftmerge* to combine the light curves from both the observations in a given energy range from each exposure-IDs into a single light curve. Similarly, we have used the combined the ME light curves in 10-30 keV obtained from both the *Insight–HXMT* observations to obtain the periodograms as shown in Figure 4. For the timing studies of 4U 2206+54 with *AstroSat* , we have followed similar procedure. We have combined the light curves obtained at similar energies of LAXPC -1 from both the *AstroSat* observations to generate a single light curve. Similarly, the light curves are obtained from SXT and CZTI observed energy ranges. These light curves are further used to search

for pulsations and generate pulse profiles in different energy range.

3.1. Determination of NS spin period

The ~ 5500 s long spin-period of the pulsar in 4U 2206+54 has previously been known to show long-term spin down (Reig et al. 2012; Wang 2013; Torrejón et al. 2018). In order to determine the present value of its NS spin period in 4U 2206+54 and its possible trend, we have extracted a light curve in 5 – 10 keV from the LAXPC-1 observation. From this a background subtracted and barycentric corrected source light curve has been used to estimate the pulsar spin-period. The *AstroSat* /LAXPC observations of 4U 2206+54 span a total duration of 88.4 msec of which the effective pointed observation on source is ~ 40.7 msec after applying the GTI selection. We have shown the 5–10 keV light curve of 4U 2206+54 in the inset of Fig.3 which is also binned with 100 sec time bin. It can be seen from the figure that, the observed data is sparse and discontinuous containing data gaps to avoid the SAA Anomaly. This is also the case with *NuStar* observations of 4U 2206+54 (Torrejón et al. 2018).

Due to the long spin period of the pulsar, it can be seen from the inset of Fig. 3 that, the *AstroSat* observations also have incomplete phase coverage and thus restricting the use of any Fourier techniques for an ab-initio search of periodicity in the light curve. Secondly after applying the GTI selection to the LAXPC observation, the individual data segment within the LAXPC observation have lesser duration than the spin period of the pulsar. Therefore we have used period finding methods like CLEAN (Roberts et al. 1987), SCARGLE (Scargle 1982; Press & Rybicki 1989), the phase dispersion minimization technique (PDM; Stellingwerf 1978) & the classical discrete Fourier transform (FT; Deeming 1975). These algorithms were a part of PERIOD (version 5.0), a time-series analysis package of the STARLINK⁹ software package (Currie et al. 2014). With the application of discrete Fourier transform method of Period04 (Lenz & Breger 2005) program, we get a periodic signal at frequency $\nu = 0.0001768967$ Hz (from *AstroSat*) and at $\nu = 0.0001885529$ Hz (from *Insight–HXMT*) observed light curves. The error on the frequency estimate is obtained within the Period04 program, wherein we have used the results from 500 Monte-Carlo simulations of the processes. Each process consists of creating a time string data based on the original time string data of the light curve. The simulated count rate is then predicted by the last fit plus Gaussian noise.

In Table 2, we show the spin-period estimates of 4U 2206+54 obtained from these procedures. We have also performed a significance analysis of the peaks obtained with

⁹ <http://starlink.eao.hawaii.edu/starlink>

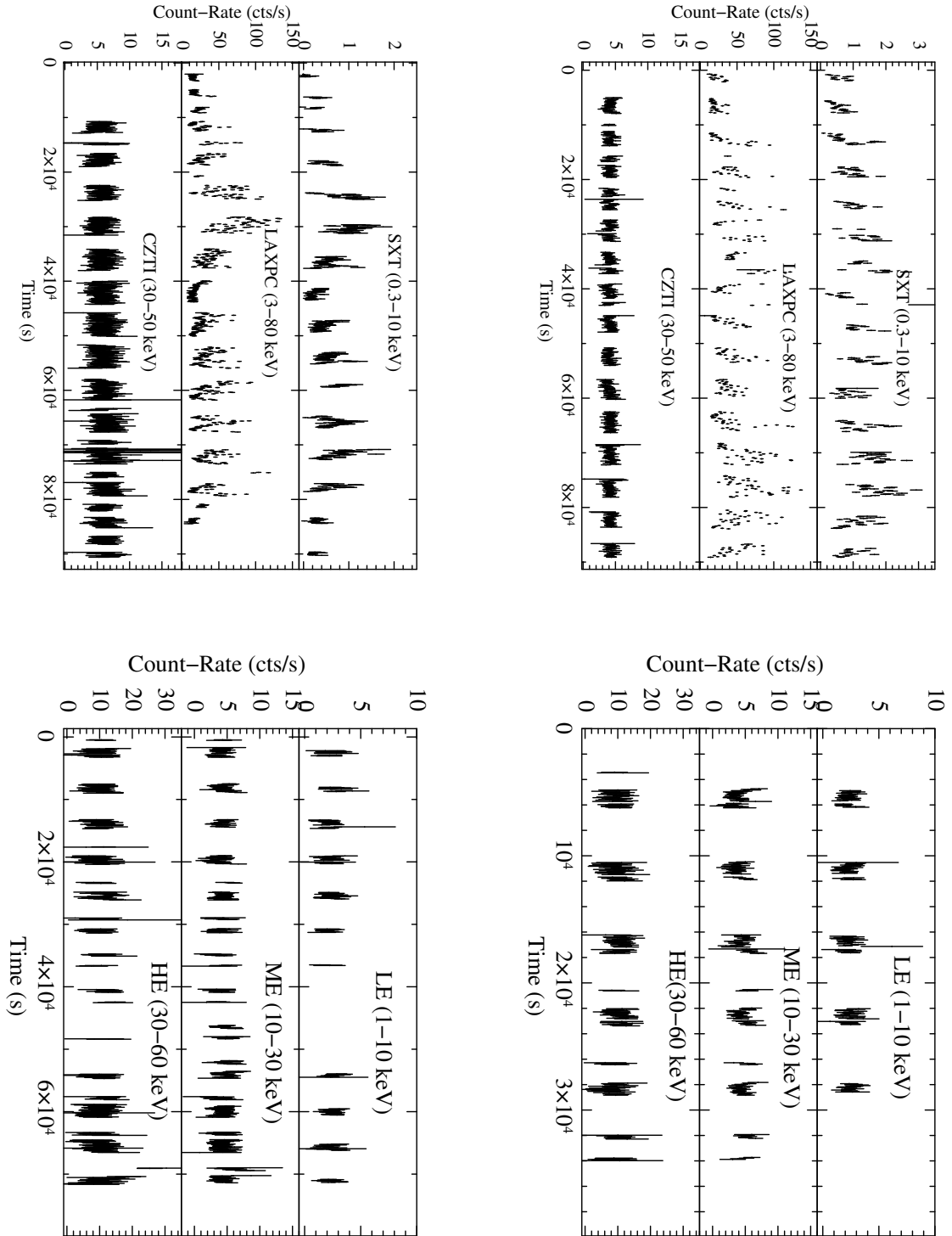


Figure 3. The light-curves of 4U 2206+54 in different energy bands obtained from *AstroSat* & *Insight-HXMT* observations. The light-curves obtained from *AstroSat* observations with OBSIDs: 9000000644 (top left), 9000000720 (top right) and from the *Insight-HXMT* observations with OBSIDs: P0305070003 (bottom left), P0305070004 (bottom right) are shown in the figure. The insets in each figure represent the X-ray energy-bands and the corresponding instruments from which the background corrected light-curves (mask weighted correction in case of *CZTI*) are obtained. The light curves are binned with a 100 sec time bin.

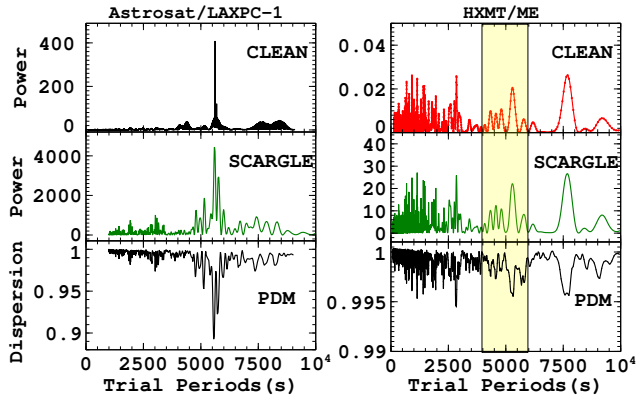


Figure 4. Periodograms from the lightcurves of 4U 2206+54 obtained using the CLEAN, SCARGLE and the PDM algorithms. The periodograms on the left are obtained from the combined *AstroSat* /LAXPC-1 observations (ObsIDs: 9000000644, 9000000720) in 3-80 keV. The periodograms on the right are obtained from the combined *Insight-HXMT* /ME observations (ObsIDs: P030507003, P030507004) in 10-30 keV. From these the estimated values of spin periods are shown in Table 2.

these procedures. The calculation of false alarm probabilities lie between 0.00 and 0.01 implying the peaks are significant with a 95% confidence. We have considered the spin period value obtained from CLEAN method as our best estimate. A comparison of recent NS spin period evolution in 4U 2206+54 from *AstroSat* & *Insight-HXMT* observations over its past 30 years evolution is shown in Fig. 5. The spin period obtained from the *AstroSat* observations shows that the pulsar is spinning up recently after reaching its slowest period of ~ 5750 sec as seen from *NuStar* observations (Torrejón et al. 2018). We note that, previously Jain et al. (2022) found the spin period to be 5648(4) s from the second *AstroSat* observation (OBSID: 9000000720) using the Lomb-Scargle periodogram method. Whereas the use of χ^2 maximization technique led them to a spin-period estimate of 5608(4) s for the same observation. It can be seen that, with the use of different period finding methods, the spin-period estimates are found to varying between 5608 s to 5652 s. This could be due to the presence of data gaps in the observed light curves (see Fig 3) leading to incomplete phase coverage of the observed signal. Secondly, this also may suppress the power of the fundamental peak in a time series data (see Torrejón et al. (2018)). This can be seen from the periodograms obtained from HXMT/ME observed lightcurves (Figure 4). Our estimate of spin period from *Insight-HXMT* observations of 4U 2206+54 further confirm the rapid spin-up of the pulsar (as can be seen in Fig.5). The latest spin-down rate of the pulsar until *NuStar* observation was $(-1.8 \pm 0.1) \times 10^{-14} \text{Hz s}^{-1}$ (Torrejón et al. 2018). The subsequent spin-up episode of the pulsar in 4U 2206+54 as observed with *AstroSat* and *Insight-HXMT*

Table 2. Estimation of spin period(s) of 4U 2206+54 from *AstroSat* and *Insight-HXMT* observations.

Instrument	Astrosat/LAXPC	HXMT/ME
OBSID	(644+720)	(7003+7004)
Method	P_{spin} (s)	P_{spin} (s)
CLEAN	5619 ± 3	5291 ± 28
SCARGLE	5653 ± 3	5291 ± 28
PDM	5627 ± 3	5319 ± 29
CHISQ	5616 ± 3	5291 ± 28
DFT (period04)	5652 ± 2	5303 ± 17
Mean	5633 ± 2	5299 ± 5
Weighted mean	5637 ± 1	5300 ± 11
Final adopted value	5619 ± 3	5291 ± 28

observations in the present work indicates a net spin-up rate of $(1.2 \pm 0.1) \times 10^{-13} \text{Hz s}^{-1}$. This is an order of magnitude higher than the long-term spin down trend of the pulsar. The previously reported spin-down rate of the pulsar were $\dot{\nu} = (-1.7 \pm 0.3) \times 10^{-14} \text{Hz s}^{-1}$ (Finger et al. 2010) and $\dot{\nu} = (-1.5 \pm 0.2) \times 10^{-14} \text{Hz s}^{-1}$ (Reig 2012).

3.2. Pulse profiles and pulse fractions

We have folded the lightcurves obtained from combined *AstroSat* observation with the estimated spin period of 5619 ± 3 s with the epoch of folding at MJD 57637.076 to obtain the pulse profiles in different energy range. In Fig. (6) these pulse profiles are shown in 0.3 – 50 keV. The pulse profiles are broadly single peaked with the appearance of narrow structures in the 0.5 – 0.7 phase bins in 0.3–5 keV. The shape and structure of the profile remains similar across different energy bands. There are no major energy dependence features seen in the pulse profiles upto 30 keV during *AstroSat* observations. The shape of the pulse profile remains same with energy upto 50 keV. At hard X-rays energies above 30 keV the pulse profiles become smooth and single peaked with the disappearance of narrow structures as seen at lower energies during the *AstroSat* observations. The pulse-profiles from *Insight-HXMT* observations are obtained from folding the HE, ME and LE lightcurves with the spin-period of 5291 ± 28 s considering the folded epoch at MJD 59132.545. These pulse profiles in different energy ranges seen with *Insight-HXMT* show marginal pulsations (Fig.6). A prominent peak at 0.7–0.8 pulse phase bins is clearly seen at 10-30 keV. Beyond which, it starts diminishing and comparable with the other structures (Fig. 7). Unlike *AstroSat* observations, we do not see clear pulsations in 30–50 keV and beyond during *Insight-HXMT* observations of 4U 2206+54.

The average pulse-fraction (PF defined as the ratio of intensity at the maximum minus the minimum of pulse profile

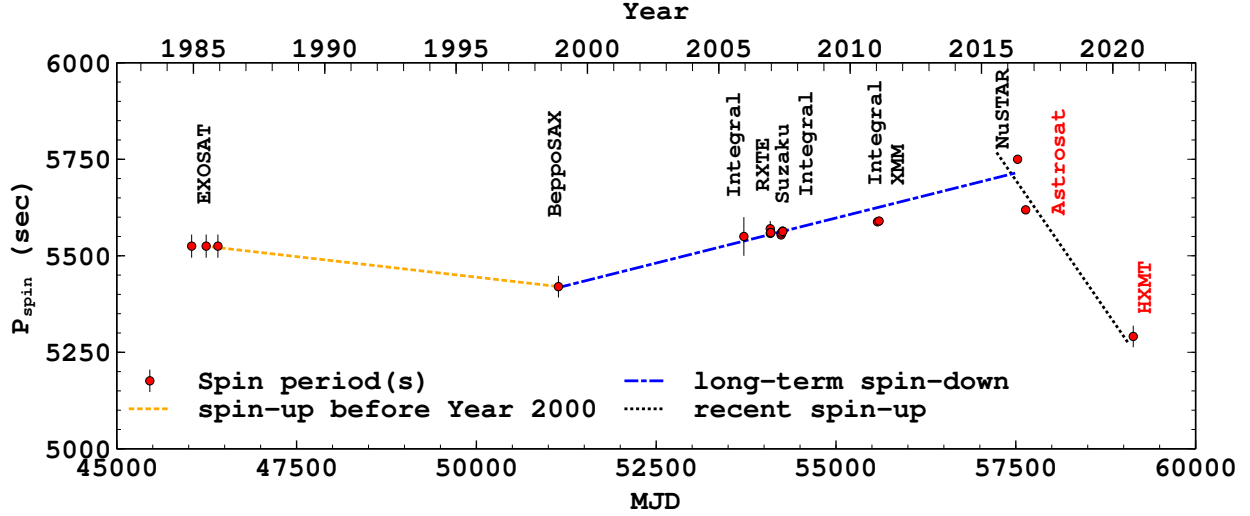


Figure 5. Long term spin period evolution of pulsar in 4U 2206+54 . The linear fit for the recent spin-up episode is obtained from *NuStar* to *Insight-HXMT* observation of 4U 2206+54 as: $P_{spin}=21202.8-0.2697 * MJD$ with an estimated pulsar spin-up rate of $(1.2 \pm 0.1) \times 10^{-13} \text{ Hz s}^{-1}$.

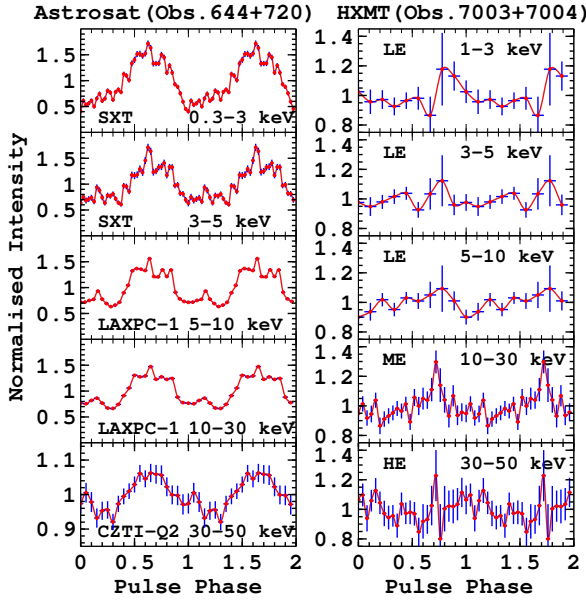


Figure 6. Comparing the energy resolved pulse profiles of 4U 2206+54 obtained from *AstroSat* (panels in left) and *Insight-HXMT* (panels in the right) observations. The pulse profiles were obtained with a folded period of 5619 sec at MJD 57637.076 with light curves obtained from *AstroSat* observations. And with a folded period of 5291 sec at MJD 59132.545 to the light curves obtained from *Insight-HXMT* observations in the respective energy bands as shown in the inset of each plot. Two complete pulse profiles are shown in each panel for the clarity.

to the maximum plus minimum intensity) is found to be 63% in soft X-rays in 0.3-3 keV . Thereby a decreasing trend upto $\sim 42\%$ in 5-10 keV . There is a marginal increase of pulse-fraction value to 47% in 10-20 keV . Subsequently, there is

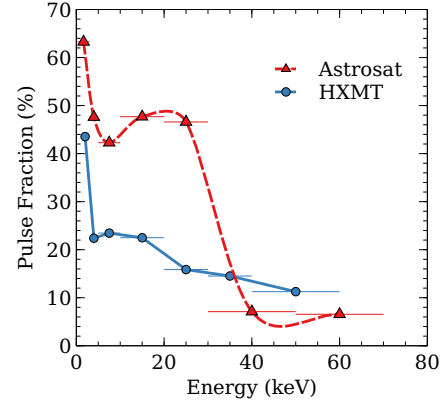


Figure 7. Pulse Fraction changes with energy as seen during *AstroSat* & *Insight-HXMT* observations of 4U 2206+54 .

a decreasing trend seen up to 30 keV with a further decline up to 7% in 50-80 keV . Beyond 30 keV the pulse-fraction is marginal (*i.e.* $< 10\%$) in hard X-rays. The changes in PF value with energy during *AstroSat* & *Insight-HXMT* observations is shown in Figure 7.

4. SPECTRAL ANALYSIS

The broad-band continuum spectra of 4U 2206+54 in 1–60 keV obtained from *AstroSat* observations is shown in Fig. 8. For this we have used the spectra obtained from *SXT* , *LAXPC* and *CZTI* .The spectra of 4U 2206+54 obtained from *Insight-HXMT* observations were found to be not suitable for spectral studies, because the spectra are mostly background dominated.

4.1. The SXT spectrum

The soft X-ray spectrum of the source from SXT observation is obtained from the merged clean event file (see section 2.1.1). For the extraction of the source spectrum we have used the XSELECT with the same region filter (i.e 10' around the source with coordinates centered at RA: 332.0162, DEC: 54.4884) as that was used earlier to extract source light curves in different energy ranges. For the PC mode observations of our source, the required SXT background spectrum file and the instrument response file as provided by the SXT instrument team has been used in our spectral analysis. An off-axis ancillary response file (ARF) that is needed during the spectral fitting has been created using the SXT Off-axis ARF Making Tool (sxtmkarf) from an input ARF file ¹⁰. For the use of SXT source spectra in spectral fitting, we have used the data in 1.0 – 7.0 keV while applying a binning scheme of having a minimum of 30 counts per bin to use χ^2 -statistics in spectral fitting.

4.2. The LAXPC spectrum

We have obtained the source and background spectra from LAXPC units as briefly mentioned in the section 2.1.2. The source spectra from the LAXPC-20 & LAXPC-30 units in the energy range of 4-30 keV has been used in our spectral analysis. We have restricted the LAXPC observed source spectra upto 30 keV beyond which, it is mostly the X-ray background. The response files of these detector units close to the epoch of observations were used from the LAXPC Response files provided by Astrosat Science Support Cell (ASSC) ¹¹.

4.3. Phase-averaged spectroscopy

The simultaneous observations of 4U 2206+54 with SXT, LAXPC and CZTI instruments onboard *AstroSat* has allowed us to explore the broad-band spectra of the pulsar 4U 2206+54. In order to study its spectral properties, we have used the X-ray spectral fitting package XSPEC (version 12.10.1) (Arnaud 1996) to simultaneously fit the SXT, LAXPC and CZTI spectra in the energy interval of 1-60 keV. The spectra of 4U 2206+54 has been fitted with various empirical models such as: a cutoff power-law model (CUTOFFPL), a high-energy cutoff powerlaw (HIGHECUT), and a two component cutoff power-law model having negative and positive exponential cutoff (NPEX)(Mihara et al. 1995). In our spectral analysis we have used the above models, allowing a 3% systematic error in the fitting. These models are generally found useful in describing the spectra of accretion-powered X-ray pulsars in a broad luminosity range. To account for the galactic absorption of X-rays along the direction of the source, we have used the photoelectric absorption model component

Table 3. Best-fitting spectral parameters with 2σ (90%) errors obtained from *AstroSat* observations (ObsID: 9000000644, 9000000720) of 4U 2206+54. The 1-60 keV composite spectra is fitted with an empirical continuum model such as a power law model with a High-energy cutoff (i.e. HIGHECUT).

Model	Parameters	9000000644	9000000720
TBABS	N_{H1} ($(10^{22} \text{ cm}^{-2})$)	3.1 ± 0.2	1.7 ± 0.1
TBPCF	N_{H2} ($(10^{22} \text{ cm}^{-2})$)	11.4 ± 1.4	-
	Cvr. Frac.	0.66 ± 0.04	-
POWERLAW	Γ	1.6 ± 0.1	1.2 ± 0.1
	$Norm_{PL}$	0.073 ± 0.014	0.017 ± 0.002
HIGHECUT	E_{cut} (keV)	7.8 ± 0.6	4.1 ± 0.4
	E_{fold} (keV)	18.7 ± 2.2	13.5 ± 0.7
	$F_{1-7 \text{ keV}}^a$	3.45	1.20
	$F_{7-30 \text{ keV}}^a$	1.86	2.35
	$F_{30-60 \text{ keV}}^a$	0.67	0.78
	$L_x^b(1-60 \text{ keV})$	6.5	4.5
	$\chi_v^2(\text{d.o.f})$	1.01 (652)	1.10(606)

Notes: ^a : Absorption corrected flux in unit of $\text{erg cm}^{-2} \text{ s}^{-1}$;

^b : The 1–60 keV X-ray luminosity in the units of $10^{35} \text{ erg s}^{-1}$ assuming a distance of (3.7 ± 0.4) kpc to the source.

(TBABS) along with the above empirical continuum models in our spectral fitting.

We have seen that the above mentioned continuum models fit the spectra well. We have therefore chosen the HIGHECUT model explain the *AstroSat* spectra of 4U 2206+54. This model gives fits with better statistics with $\chi^2(\text{dof})$ of 658.36 (652) and 669.7 (606) respectively for the first and second *AstroSat* observations (ObsID: 9000000644, 9000000720). The CUTOFFPL model applied to the phase-averaged spectra, results in comparable $\chi^2(\text{dof})$ values of 639.4(627) and 612.5(582) respectively for the above *AstroSat* observations.

From the spectral residual, we find that the spectra from first *AstroSat* observation (i.e. ObsID: 9000000644) require a partial absorbed component in addition to the galactic absorption component to better fit the spectra at soft X-rays. Whereas, for the second *AstroSat* observation, we do not require any partial absorbed component at low X-ray energies. The significance of additional absorbed component along with the high-energy Cutoff power law (HIGHECUT) continuum model can be seen from comparing the values of chi square fit statistics and degrees of freedom with and without the extra absorption component. We find that, with the inclusion of absorbed component (TBPCF) results in a Chi-squared value of 658.36 with 652 degrees of freedom. Whereas without the absorbed component, the Chi squared value of fit statistic is 752.39 with 654 degrees of freedom (d.o.f). A ftest compar-

¹⁰ http://www.tifr.res.in/~astrosat_sxt/dataanalysis.html

¹¹ <http://astrosat-ssc.iucaa.in/?q=laxpcData>

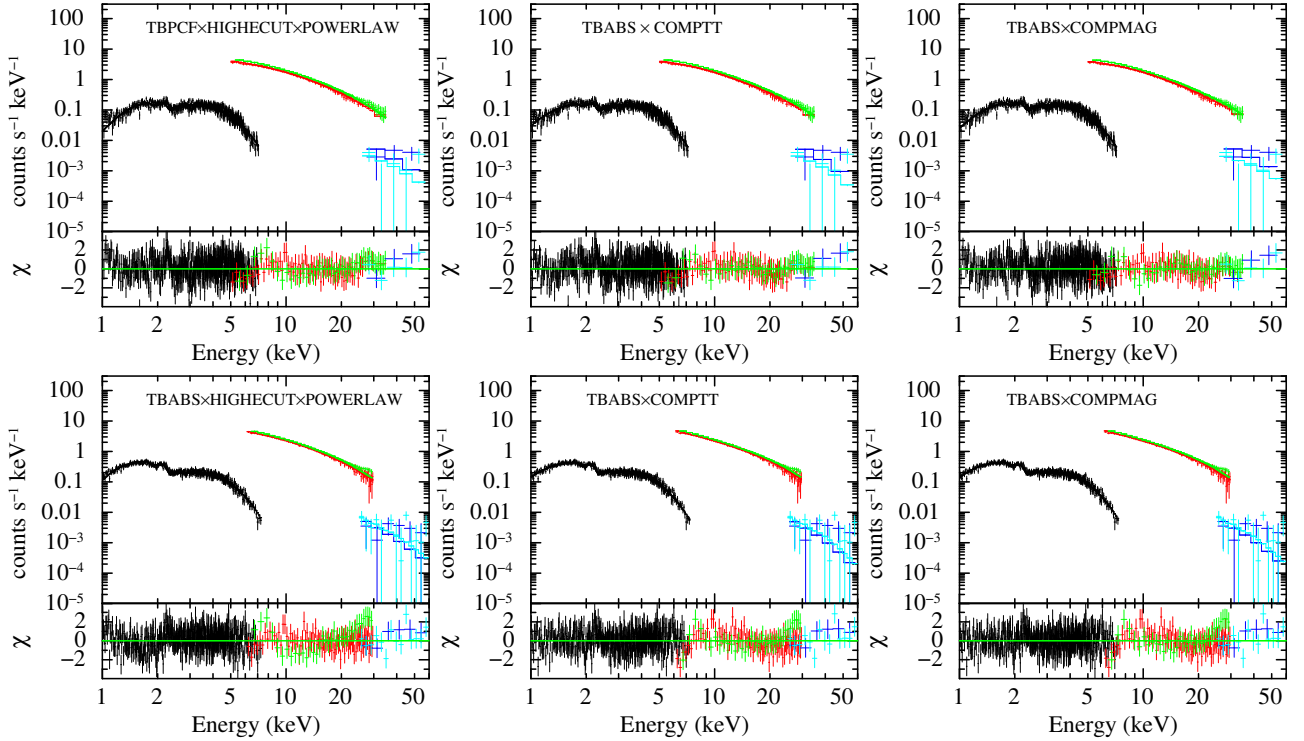


Figure 8. The broadband phase averaged spectra of 4U 2206+54 in 1–60 keV obtained from the *AstroSat* /*SXT* (1–7 keV), *LAXPC* (7–30 keV) and *CZT* (30–60 keV) from observations with OBSIDs: 9000000644 (figures in top panels) and 9000000720 (figures in bottom panels). The spectra is best fitted with models such as: an absorbed high-energy cutoff continuum model and Comptonization models such as: *COMP MAG*, *COMP TT*. The second panels in each of the figure shows the spectral residual obtained after the best-fitted continuum model.

ison of these two chi-square values yields F-statistic value of 46.56 with a very low *f*test probability of 1.255×10^{-19} . A similar need of additional absorbed component is also seen with the *CUTOFFPL* continuum model while fitting the broadband spectra of *AstroSat* observation (ObsID: 9000000644). In case of best fitted *CUTOFFPL* model we have obtained the chi-squared value of 639.42 with 627 d.o.f with the additional absorbed component and the chi-squared value of 772.86 for a 629 d.o.f. without the absorbed component. The subsequent *f*test comparison of *CUTOFFPL* models for the inclusion of absorbed component yields a very low *F*test probability of 1.56×10^{-26} with a *F* statistic value of 65.42. Given the low values of *f*test probability, it is reasonable to explain the broadband spectra with the additional absorbed component.

We choose the *HIGHECUT* model to explain the phase averaged spectra of both the *AstroSat* observations in 1–60 keV. The best fitted spectral parameters obtained from the model are shown in Table 3 along with the absorption corrected source X-ray flux estimates in soft and hard X-ray energy bands. The uncertainties in the spectral parameter estimates are quoted at 1σ confidence level for one parameter of interest. In the first panels of Fig. 8, we show the 1–60 keV unfolded spectrum of the source along with the best-fitted high-energy cutoff continuum model. It can be seen from Table 3 that, the absorption corrected soft X-ray flux in 1–7 keV from first *AstroSat* observation is $3.45 \times$

$10^{-10} \text{ erg cm}^{-2} \text{ s}^{-1}$ comparatively high than that of the second observation by a factor of more than 2. Whereas the hard X-ray flux in 7–30 keV and 30–60 keV are of similar magnitude in both the *AstroSat* observations. Apart from these, the spectral parameter values such as: cutoff-energy E_{cut} , folding-energy E_{fold} , and the powerlaw spectral index (Γ) are found to be higher for the first *AstroSat* observation compared to the second observation. We note that, using only the *LAXPC* spectra in 3–30 keV of above *AstroSat* observations, Jain et al. (2022) have explained the spectra with a *HIGHECUT* model. Whereas, our broadband spectral coverage in 1–60 keV allowed us to identify additional absorption in soft X-rays of the first *AstroSat* observation.

Secondly, we have seen that, only from the *LAXPC* data of first *AstroSat* observation, Jain et al. (2022) have reported a detection of broad emission line around 7 keV. However, from our spectral fitting of the same *LAXPC* observations along with *SXT* observations in 1–7 keV and *CZTI* observations in 30–60 keV, we do not observe any such line emission feature around 7 keV. In the second *AstroSat* observation also we do not find any significant line emission. The non-detection of any line emission in the broadband spectral fitting for the second observation agrees with the spectral results of Jain et al. (2022). Therefore we have not included any emission line component in the spectral fitting of 4U 2206+54 spectra. In the hard X-rays, from *AstroSat* ob-

Table 4. Best-fit parameters of the Comptonization models TBABS×COMPTT and TBABS×COMPAG for 4U 2206+54 broad-band spectra in 1-60 keV obtained from *AstroSat* observations with observation-IDs 9000000644 & 9000000720 respectively. In case of COMPAG model, we have fixed the model parameters $\eta=1$, $\beta_0=0.05$, $r_0=0.25$ and $A=0.5$ for both the *AstroSat* observations.

Model	Parameter	9000000644	9000000720
TBABS	N_H (10^{22} cm $^{-2}$)	$1.62^{+0.06}_{-0.06}$	$0.82^{+0.05}_{-0.05}$
COMPAG	kT_{bb} (keV)	$1.56^{+0.03}_{-0.02}$	$0.89^{+0.02}_{-0.02}$
	kT_e (keV)	$14.9^{+5.6}_{-1.0}$	$7.1^{+0.9}_{-0.5}$
	τ	$0.22^{+0.01}_{-0.04}$	$0.36^{+0.01}_{-0.01}$
	Norm	$28.7^{+9.6}_{-5.3}$	$57.8^{+3.9}_{-3.8}$
	$F_{1-7\text{ keV}}^a$	1.77	1.05
	$F_{7-30\text{ keV}}^a$	1.8	2.35
	$F_{30-60\text{ keV}}^a$	0.78	0.40
	χ^2_{ν} (d.o.f)	0.98 (655)	1.02(606)
TBABS	N_H (10^{22} cm $^{-2}$)	$1.01^{+0.12}_{-0.11}$	$0.59^{+0.07}_{-0.06}$
COMPTT	kT_0 (keV)	$1.33^{+0.05}_{-0.05}$	$0.76^{+0.02}_{-0.02}$
	kT_e (keV)	$8.05^{+2.14}_{-1.08}$	$6.79^{+0.59}_{-0.46}$
	τ	$3.06^{+0.42}_{-0.56}$	$3.63^{+0.23}_{-0.24}$
	Norm	$(6.9 \pm 0.7) \times 10^{-3}$	$(4.5 \pm 0.1) \times 10^{-3}$
	$F_{1-7\text{ keV}}^a$	1.7	1.0
	$F_{7-30\text{ keV}}^a$	1.8	2.35
	$F_{30-60\text{ keV}}^a$	0.64	0.44
	χ^2_{ν} (d.o.f)	0.99 (668)	1.02 (606)

^a In units of 10^{-10} erg cm $^{-2}$ s $^{-1}$.

served spectra, we do not see any signature of cyclotron line emission at 35 keV, that was anticipated earlier during *Bep-poSAX* observations (Masetti et al. 2004). The non-detection of cyclotron line is also reported from earlier from *INTEGRAL* observations (Wang 2013) and recent *NuStar* observations of the pulsar (Torrejón et al. 2018).

Apart from explaining the phase averaged spectra of 4U 2206+54 with empirical continuum models, we have also studied the spectra with application of Comptonization models. Previous studies have shown that, the physical models based on Comptonization also provide good fits to the data (Masetti et al. 2004; Reig et al. 2009; Torrejón et al. 2018). Therefore we have also followed this approach to explain the *AstroSat* observed spectra of 4U 2206+54 in 1-60 keV. In our spectral fitting with these models, we find that any additional blackbody component is not needed at soft X-rays to explain broad phase averaged spectra. For both the *AstroSat* observed spectra of 4U 2206+54, we find that the application of COMPTT and COMPAG Comptonization models could fit the spectra well. The COMPTT model applied to first *As-*

troSat observation (*i.e.* ObsID: 9000000644) has a χ^2 (dof) of 667.9(668) and for the second observation (*i.e.* ObsID: 9000000720) has a χ^2 (dof) of 617.9(606). The COMPAG model similarly yields a χ^2 (dof) of 642(655) and 616.5(606) for first and second observations respectively. To account for the galactic absorption along the line of sight, we have used TBABS model with the ISM abundances and photoionization cross sections set to wilm abundances (Wilms et al. 2000). We find that, the average H1 column density (NH) estimated through H14Pi map (H14PI Collaboration et al. 2016) for the sky position of 4U 2206+54 is 0.55×10^{22} cm $^{-2}$. From the best fitted spectral parameters obtained from Comptonization models with TBABS component as mentioned in Table 4, we find that the estimated column density is similar to the value obtained from H14Pi map. For the first *AstroSat* observation, however, we see a slight increase of N_H values albeit with higher values of blackbody seed photon temperature (kT_0). The absorption corrected flux for the pulsar in 1–7 keV, 7–30 keV and 30–60 keV obtained from *SXT*, *LAXPC* and *CZTI* observed spectra respectively are also estimated using best-fitted Comptonization models. The estimated flux values show similar values in both the Comptonization models. The net flux in 1-60 keV during first observation is higher compared to the second *AstroSat* observation of 4U 2206+54.

The COMPAG model (Farinelli et al. 2012a) assumes a cylindrical accretion geometry for the matter accreting onto the polar cap of a magnetized neutron star. Numerically, it solves the radiative transfer equations, assuming a cylindrical accretion onto a magnetized neutron star where both the thermal and bulk Comptonization of seed photons occur. The seed photon spectrum is primarily of blackbody in nature with an exponential distribution within the accretion column. Farinelli et al. (2012a) further states that the COMPAG model generally holds good for an optical depth $\tau \geq 1$ as the model is based on Fokker-Planck approximation of the radiative transfer equation. In our best fitted spectra of 4U 2206+54 with COMPAG, however, we obtain τ values within a factor of 3 to unity. This has been explained in case of XTE J1739–302 (Farinelli et al. 2012b) that, such a scenario would arise for an inefficient diffusion of photons along the column axis. Therefore the photons may efficiently propagate perpendicular the column axis. The other possibility is that, emission being anisotropic due to strong magnetic field of the neutron star.

The possibility of high magnetic field strength of magnetar nature (Reig et al. 2012; Wang 2013) further supports this in case of 4U 2206+54. Since the other physical parameter results such as electron temperature (kT_e) and blackbody photon temperature (kT_{bb}) are consistent within the estimated 1σ errors with that from COMPTT model parameter values (*i.e.* kT_e and kT_0), these variations can be discussed

reasonably using COMPAG physical model. From the Comptonization model parameters, we notice that, the soft photon source temperature (kT_{bb}) during the first *AstroSat* observation is substantially higher compared to thesecond *AstroSat* observation. The hotter blackbody temperature is observed in 4U 2206+54 spectra of first *AstroSat* observation with both COMPAG and COMPTT model. In the spectral fitting with COMPAG model, we have fixed some of the model parameter values such as the index of velocity profile ($\eta = 1$), terminal velocity at the NS surface ($\beta_0 = 0.05$), NS albedo $A=1$ and the radius of accretion column in units of the neutron star Schwarzschild radius as: $r_0=0.25$. This corresponds to ~ 1 km for a $1.4M_\odot$ mass neutron star. Alternatively, from the normalization constant $\left(\frac{R_{km}}{d_{10kpc}}\right)^2$ of the COMPAG model, the estimated soft photons source radius R_{km} varies from ~ 2.0 to 2.8 km during the two epochs of *AstroSat* observations. We have noticed that, by increasing the value of r_0 from 0.25 to 0.5 , there is no significant change in the observed χ^2 -value. The other model parameters such as the electron temperature (kT_e), the blackbody temperature (kT_{bb}) and the accretion column optical depth (τ) are kept free. The lesser value of τ , the vertical column optical depth in COMPAG model is due to electron cross-section being less than that of the Thomson cross-section σ_T by a factor of 1000 . This is due to inclusion of an energy-independent correction term which reduces σ_T for photons propagated along the magnetic field (see Farinelli et al. 2012a and references therein).

5. DISCUSSION

The rapid spin changes of the slow rotation pulsar in 4U 2206+54, make it one of the interesting source to test the theories of spin-period evolution in long-period X-ray pulsars. In this paper, we have compared the recent changes in the pulsar spin period with those of previous studies. In the high mass X-ray binary system 4U 2206+54 the ~ 5500 sec X-ray pulsations have been previously been interpreted as the NS spin period (Finger et al. 2010) present in the system. During 2005–2011, the monitoring of the source with *INTEGRAL* has shown a long-term spin-down trend with the pulsar spin period from ~ 5558 to ~ 5588 s (Wang 2013). From the *AstroSat* observations of the pulsar, we estimate the present spin-period of 5619 ± 3 sec. A recent *NuStar* observation of the source (i.e at MJD 57525.41) taken prior to *AstroSat* observation report a spin period estimate of 5750 ± 3 sec (Torrejón et al. 2018). We note that the previous studies of 4U 2206+54 have confirmed the continuing long term spin-down trend of the pulsar (Torrejón et al. 2018; Wang 2013; Reig et al. 2012, 2009). However from our studies, the recent spin period estimate of the pulsar from *AstroSat* observations hints that the pulsar is showing a spin-up episode after its 20-year long spin-down process. We note that, the pulsar in 4U 2206+54, after reaching thus far its slowest

pulse period of ~ 5750 sec as seen from *NuStar* (Torrejón et al. 2018), has recently been transiting to a spin-up phase. Between these two epochs (i.e *NuStar* and *AstroSat* observations separated by ~ 112 days apart) we found that the pulsar in 4U 2206+54 is transiting to a spin-up episode at a rate of 4.3×10^{-13} Hz s^{-1} . Before this a look at the previous episodes of spin-period variations in 4U 2206+54 shows that, the long term spin-down of the pulsar had continued at a rate $\dot{\nu} \sim -(1.8 \pm 0.1) \times 10^{-14}$ Hz s^{-1} (Torrejón et al. 2018). The recent *Insight-HXMT* observations of 4U 2206+54 further confirm the significant spin-up of the slow rotating pulsar (see Fig.5). The resulting spin-up from the latest *NuStar* observation to the present *Insight-HXMT* observations indicate a spin-up rate of $\dot{\nu} = (1.2 \pm 0.1) \times 10^{-13}$ Hz s^{-1} (see Figure 5). This indicates that, the NS undergoing a strong positive torque even at relatively low X-ray luminosity $L_x \leq 6.5 \times 10^{35}$ erg s^{-1} (see in Table 3).

Such a scenario can occur in a settling quasi-spherical accretion regime (Shakura et al. 2012). In this regime, the optical companion star underfills its Roche lobe with no possibility of formation of an accretion disc around the NS. The radial velocity of accreting plasma is subsonic. As the net X-ray flux is low enough at the Bondi radius, the accreting shocked matter at the NS magnetosphere remain hot with the formation of a hot quasi-static shell. Due to temperature gradients across the shell, large scale convective motions appear across the shell. The subsonic settling of accretion occurs at the magnetosphere via instabilities eventually the matter accreting onto the NS. The subsonic quasi-static shell mediates the removal of angular momentum from the NS magnetosphere in settling accretion (Shakura et al. 2012).

The temperature of the matter in the shell will be high (of the order of Virial temperature, Davies & Pringle 1981). In case of 4U 2206+54, the high values of $kT_e \sim 7-15$ keV imply hot matter around the NS in a quasi-static shell. By comparing the kT_e values from the first and second *AstroSat* observations, we see a substantial Compton cooling of plasma. This could then facilitate the plasma to enter the NS magnetosphere from a hot envelope. Depending upon the sign of angular velocity difference between accreting matter and the magnetospheric boundary, the neutron star may spin-up or spin-down as its magnetosphere interacts with the hot envelope (or quasi-static shell). The settling accretion and formation of hot convective shell occurs at X-ray luminosity below a critical value of $\sim 4 \times 10^{36}$ erg s^{-1} (Davies & Pringle 1981; Shakura et al. 2012) at which the angular momentum from the neutron star magnetosphere can be transferred away through the shell by turbulent viscosity and convective motions. The lower X-ray luminosity value noted in 4U 2206+54 from *AstroSat* observations along-with higher plasma temperature, further confirm that, the NS underwent a settling accretion regime with possibly a short term spin-

up episode. We observe that, the pulsar in 4U 2206+54 has shown previously strong spin-down episode (Torrejón et al. 2018) followed by present transition to a short-term spin-up phase during *AstroSat* and *Insight–HXMT* observations. This suggests that, the pulsar is not in equilibrium.

Rapid spin-up episodes on top of the long-term spin-down trend have also been observed in other long period pulsars such as GX 301–2 (Pravdo & Ghosh 2001; Doroshenko et al. 2010; Ding et al. 2021). These changes reflect that the pulsar is entering into a strong coupling regime (Shakura et al. 2012) temporarily. During which, the accreting matter at the Alfvén radius (R_A) couples with the magnetosphere acquiring angular velocity of the neutron star. The accreting matter as it falls onto the NS, it returns the angular momentum to the NS acquired at R_A via the strong magnetic field. This leads to a significant spin-up of the pulsar. During the recent spin-down state of the pulsar, Torrejón et al. (2018) have obtained a lower limit on the NS dipole magnetic moment of the pulsar to be $\mu > 10^{31}$ G cm³, where they have assumed the pulsar is in spin-equilibrium with the X-ray luminosity much smaller than the equilibrium luminosity, neglecting the spin-up torque at the spin-down stage. The dipole magnetic field of a wind-fed NS as per the spherical settling accretion theory (Popov & Turolla 2012), can be estimated as:

$$B_{12} \sim 8.1 \dot{M}_{16}^{\frac{1}{3}} V_{300}^{-\frac{11}{3}} \left(\frac{P_{1000}}{P_{orb,300}} \right)^{\frac{11}{12}}, \quad (1)$$

where the mass accretion rate \dot{M}_{16} is in units of 10^{16} g s⁻¹, the stellar wind velocity V_{300} is in units of 300 km s⁻¹, the spin-period, P_{1000} is in units of 1000 sec and the orbital period is in units of 300 d as $P_{orb,300}$.

From the *AstroSat* observed source luminosity of 4U 2206+54 in 1-60 keV, *i.e.* $L_x \sim 6.5 \times 10^{35}$ erg s⁻¹, we obtain the mass accretion rate of $\dot{M}_{16} \sim 0.35$. The stellar wind velocity in 4U 2206+54 is very slow with $V_{300} \sim 1.17$ (Ribó et al. 2006; Reig et al. 2012). Using the above values and the present spin-period estimate of the pulsar from *Insight–HXMT* observations as, $P_{1000} = 5.291$, we obtain an estimate of the pulsar magnetic field in 4U 2206+54 using equation 1 as: $B = 3.6 \times 10^{14}$ G for an orbital period of $P_{orb,300} = 0.031$ (Ribó et al. 2006) and alternatively $B = 1.85 \times 10^{14}$ G if we consider $P_{orb,300} = 0.064$. The above two possible binary orbital modulations in case of 4U 2206+54 were considered due to Ribó et al. (2006) found $P_{orb} = 9.5$ d and later a 19d modulation was suggested by Corbet et al. (2007). Nevertheless, it is interesting to note that, with an orbital period of 9.5d, 4U 2206+54 has the shortest orbital period among the known HMXBs (Hambarayan et al. 2022). Considering the NS surface magnetic field as $B = 2\mu/R^3 \geq 1.85 \times 10^{14}$ G, where R is the NS radius and μ is NS dipole magnetic moment. we obtain $\mu > 9.25 \times 10^{31}$ G cm³. These estimates agree with the results obtained in Torrejón et al. (2018),

where the spin-up torque has been ignored while estimating the NS dipole magnetic moment in a quasi-spherical settling accretion scenario.

As per the quasi-spherical settling accretion theory, the equilibrium period of an X-ray pulsar is determined as (Shakura et al. 2018):

$$P_{eq} = 1000 [s] \mu_{30}^{12/11} \left(\frac{P_b}{10d} \right) \dot{M}_{16}^{-4/11} V_8^4, \quad (2)$$

where the NS dipole magnetic moment μ_{30} is in units of 10^{30} G cm³, and the stellar wind velocity v_w is in units of 10^8 cm s⁻¹ or *i.e.* V_8 in units of 1000 km s⁻¹. For a comparison, in case of 4U 2206+54, using $v_w = 350$ km s⁻¹ *i.e.* $V_8 = 0.35$ (Ribó et al. 2006) and $P_{orb} = 9.5$ d, $\mu_{30} = 9.25 \times 10^{31}$ G cm³ (as obtained above), we find the pulsar equilibrium period is of $P_{eq} = 2823$ s. Whereas in a standard accretion disk accretion case, the equilibrium period (Shakura et al. 2018) would be determined from :

$$P_{eq,d} \approx 10[s] \mu_{30}^{6/7} \dot{M}_{16}^{-3/7}. \quad (3)$$

In case of 4U 2206+54, it is estimated to be $P_{eq,d} = 760$ s. In either scenario, it clearly demonstrates the fact that, 4U 2206+54 is a non-equilibrium pulsar. The lack of any CRSF feature in the hard X-ray spectra of 4U 2206+54 from the *AstroSat* observations, along with the indication of high-magnetic field of the pulsar, $B > 10^{14}$ G as shown above, (see also Torrejón et al. 2018; Wang 2013; Reig et al. 2012) hints at a magnetar field strength of the long-period pulsar in 4U 2206+54.

6. SUMMARY AND CONCLUSION

We have studied the recent spin-period evolution and spectral changes in the long-period pulsar in 4U 2206+54 using *AstroSat* and *Insight–HXMT* observations. These studies reveal that, the pulsar is showing a rare spin-up episode, with a short-term spin-up rate of $\dot{\nu} = 4.3 \times 10^{-13}$ Hz s⁻¹ from *NuStar* to *AstroSat* observations. The net spin-up rate from *NuStar* to *Insight–HXMT* observation gradually decreases to $\dot{\nu} = 1.2 \times 10^{-13}$ Hz s⁻¹. The phase-averaged spectral studies with Comptonization models such as `COMPTT` and `COMPAG` reveal a hotter soft-photon source region varying in size of 2 – 2.8 km near the pulsar. The net X-ray luminosity of the pulsar in 1-60 keV is $\leq 6.5 \times 10^{35}$ erg s⁻¹ as seen from *AstroSat*. In a quasi-spherical settling accretion scenario, this results in a formation of hot convective and quasi-static shell around the NS. The convective motions in the shell regulates the angular momentum transfer from the NS magnetosphere that may result in a spin-up of the pulsar. A comparison of present spin-period value with the equilibrium spin period of the pulsar obtained in different accretion regimes shows that pulsar is not in equilibrium. The non-detection

of any CRSF feature in 1-60 keV along-with the possibility of strong magnetic field NS in 4U 2206+54 as per quasi-spherical settling accretion imply the NS of magnetar field strength in 4U 2206+54 . Given the low X-ray luminosity of the pulsar and slow and marginal pulsations, the present spin-up episode can be better explored with future observations with the hard X-ray telescopes like *NuStar* , *AstroSat* and *Insight-HXMT* .

ACKNOWLEDGMENTS

We are grateful to the referee for the detailed comments. This work is supported by the the NSFC (No. 12133007) and

National Key Research and Development Program of China (Grants No. 2021YFA0718503). This work has made use of data from the Insight-HXMT mission, a project funded by China National Space Administration (CNSA) and the Chinese Academy of Sciences (CAS). This work has performed utilizing the calibration data-bases and auxiliary analysis tools provided by AstroSat-SXT team and also used the data from the Soft X-ray Telescope (SXT) developed at TIFR, Mumbai.

REFERENCES

- Agrawal, P. C., Yadav, J. S., Antia, H. M., et al. 2017, *Journal of Astrophysics and Astronomy*, 38, 30
- Arnaud, K. A. 1996, in *Astronomical Society of the Pacific Conference Series*, Vol. 101, *Astronomical Data Analysis Software and Systems V*, ed. G. H. Jacoby & J. Barnes, 17
- Bhalerao, V., Bhattacharya, D., Vibhute, A., et al. 2017, *Journal of Astrophysics and Astronomy*, 38, 31
- Bhattacharya, D., & van den Heuvel, E. P. J. 1991, *PhR*, 203, 1
- Blay, P., & Reglero, V. 2012, in *Proceedings of “An INTEGRAL view of the high-energy sky (the first 10 years)” - 9th INTEGRAL Workshop and celebration of the 10th anniversary of the launch (INTEGRAL 2012)*. 15-19 October 2012. *Bibliothèque Nationale de France*, 12
- Blay, P., Reig, P., & Reglero, V. 2014, in *Multifrequency Behaviour of High Energy Cosmic Sources*, 215–221
- Cao, X., Jiang, W., Meng, B., et al. 2020, *Science China Physics, Mechanics, and Astronomy*, 63, 249504
- Chen, Y., Cui, W., Li, W., et al. 2020, *Science China Physics, Mechanics, and Astronomy*, 63, 249505
- Corbet, R. H. D., Markwardt, C. B., & Tueller, J. 2007, *ApJ*, 655, 458
- Currie, M. J., Berry, D. S., Jenness, T., et al. 2014, in *Astronomical Society of the Pacific Conference Series*, Vol. 485, *Astronomical Data Analysis Software and Systems XXIII*, ed. N. Manset & P. Forshay, 391
- Davies, R. E., & Pringle, J. E. 1981, *MNRAS*, 196, 209
- Deeming, T. J. 1975, *Ap&SS*, 36, 137
- Ding, Y. Z., Wang, W., Epili, P. R., et al. 2021, *MNRAS*, 506, 2712
- Doroshenko, V., Santangelo, A., Suleimanov, V., et al. 2010, *A&A*, 515, A10
- Farinelli, R., Ceccobello, C., Romano, P., & Titarchuk, L. 2012a, *A&A*, 538, A67
- Farinelli, R., Romano, P., Mangano, V., et al. 2012b, *MNRAS*, 424, 2854
- Finger, M. H., Ikhsanov, N. R., Wilson-Hodge, C. A., & Patel, S. K. 2010, *ApJ*, 709, 1249
- Hambaryan, V., Stoyanov, K. A., Mugrauer, M., et al. 2022, *MNRAS*, 511, 4123
- HI4PI Collaboration, Ben Bekhti, N., Flöer, L., et al. 2016, *A&A*, 594, A116
- Jain, C., Yadav, A., & Sharma, R. 2022, *Journal of Astrophysics and Astronomy*, 43, 101
- Lenz, P., & Breger, M. 2005, *Communications in Asteroseismology*, 146, 53
- Liu, C., Zhang, Y., Li, X., et al. 2020, *Science China Physics, Mechanics, and Astronomy*, 63, 249503
- Masetti, N., Dal Fiume, D., Amati, L., et al. 2004, *A&A*, 423, 311
- Mihara, T., Makishima, K., & Nagase, F. 1995, in *American Astronomical Society Meeting Abstracts*, Vol. 187, *American Astronomical Society Meeting Abstracts*, 104.03
- Negueruela, I., & Reig, P. 2001, *A&A*, 371, 1056
- Popov, S. B., & Turolla, R. 2012, *MNRAS*, 421, L127
- Pravdo, S. H., & Ghosh, P. 2001, *ApJ*, 554, 383
- Press, W. H., & Rybicki, G. B. 1989, *ApJ*, 338, 277
- Ramadevi, M. C., Ravishankar, B. T., Sitaramamurthy, N., et al. 2017a, *Journal of Astrophysics and Astronomy*, 38, 32
- Ramadevi, M. C., Seetha, S., Bhattacharya, D., et al. 2017b, *Experimental Astronomy*, 44, 11
- Rao, A. R., Bhattacharya, D., Bhalerao, V. B., Vadawale, S. V., & Sreekumar, S. 2017a, *Current Science*, 113, 595
- Rao, A. R., Patil, M. H., Bhargava, Y., et al. 2017b, *Journal of Astrophysics and Astronomy*, 38, 33
- Reig, P. 2012, in *Astronomical Society of the Pacific Conference Series*, Vol. 466, *Electromagnetic Radiation from Pulsars and Magnetars*, ed. W. Lewandowski, O. Maron, & J. Kijak, 25
- Reig, P., Torrejón, J. M., & Blay, P. 2012, *MNRAS*, 425, 595
- Reig, P., Torrejón, J. M., Negueruela, I., et al. 2009, *A&A*, 494, 1073

- Ribó, M., Negueruela, I., Blay, P., Torrejón, J. M., & Reig, P. 2006, *A&A*, 449, 687
- Roberts, D. H., Lehar, J., & Dreher, J. W. 1987, *AJ*, 93, 968
- Roy, J., Alam, M. S., Balamurugan, C., et al. 2021, *Journal of Astrophysics and Astronomy*, 42, 28
- Scargle, J. D. 1982, *ApJ*, 263, 835
- Shakura, N., Postnov, K., Kochetkova, A., & Hjalmarsdotter, L. 2012, *MNRAS*, 420, 216
- Shakura, N., Postnov, K., Kochetkova, A., & Hjalmarsdotter, L. 2018, in *Astrophysics and Space Science Library*, Vol. 454, *Astrophysics and Space Science Library*, ed. N. Shakura, 331
- Singh, K. P., Tandon, S. N., Agrawal, P. C., et al. 2014, in *Society of Photo-Optical Instrumentation Engineers (SPIE) Conference Series*, Vol. 9144, *Space Telescopes and Instrumentation 2014: Ultraviolet to Gamma Ray*, ed. T. Takahashi, J.-W. A. den Herder, & M. Bautz, 91441S
- Singh, K. P., Stewart, G. C., Chandra, S., et al. 2016, in *Society of Photo-Optical Instrumentation Engineers (SPIE) Conference Series*, Vol. 9905, *Space Telescopes and Instrumentation 2016: Ultraviolet to Gamma Ray*, ed. J.-W. A. den Herder, T. Takahashi, & M. Bautz, 99051E
- Singh, K. P., Stewart, G. C., Westergaard, N. J., et al. 2017, *Journal of Astrophysics and Astronomy*, 38, 29
- Stellingwerf, R. F. 1978, *ApJ*, 224, 953
- Tandon, S. N., Subramaniam, A., Girish, V., et al. 2017, *AJ*, 154, 128
- Torrejón, J. M., Kreykenbohm, I., Orr, A., Titarchuk, L., & Negueruela, I. 2004, *A&A*, 423, 301
- Torrejón, J. M., Reig, P., Fürst, F., et al. 2018, *MNRAS*, 479, 3366
- Urpin, V., Konenkov, D., & Geppert, U. 1998, *MNRAS*, 299, 73
- Wang, W. 2009, *MNRAS*, 398, 1428
- . 2010, *A&A*, 520, A22
- . 2013, *MNRAS*, 432, 954
- Wilms, J., Allen, A., & McCray, R. 2000, *ApJ*, 542, 914
- Yadav, J. S., Agrawal, P. C., Antia, H. M., et al. 2016, in *Society of Photo-Optical Instrumentation Engineers (SPIE) Conference Series*, Vol. 9905, *Space Telescopes and Instrumentation 2016: Ultraviolet to Gamma Ray*, ed. J.-W. A. den Herder, T. Takahashi, & M. Bautz, 99051D
- Zhang, J., Li, X., Ge, M., et al. 2020, *Ap&SS*, 365, 158